

**Supporting Information:**

# Elucidating Tuneable Ambipolar Charge Transport and Field Induced Bleaching at CH<sub>3</sub>NH<sub>3</sub>PbI<sub>3</sub>/electrolyte Interface<sup>†</sup>

*Priya Srivastava,<sup>†</sup> and Monojit Bag,<sup>\*, †, ⊥</sup>*

<sup>†</sup>Department of Physics, Indian Institute of Technology Roorkee, Roorkee, Uttarakhand 247667,  
India.

<sup>⊥</sup>Centre of Nanotechnology, Indian Institute of Technology Roorkee, Roorkee, Uttarakhand 247667,  
India.

**Corresponding Author**

\*(Monojit Bag) Email: [mbagfph@iitr.ac.in](mailto:mbagfph@iitr.ac.in)

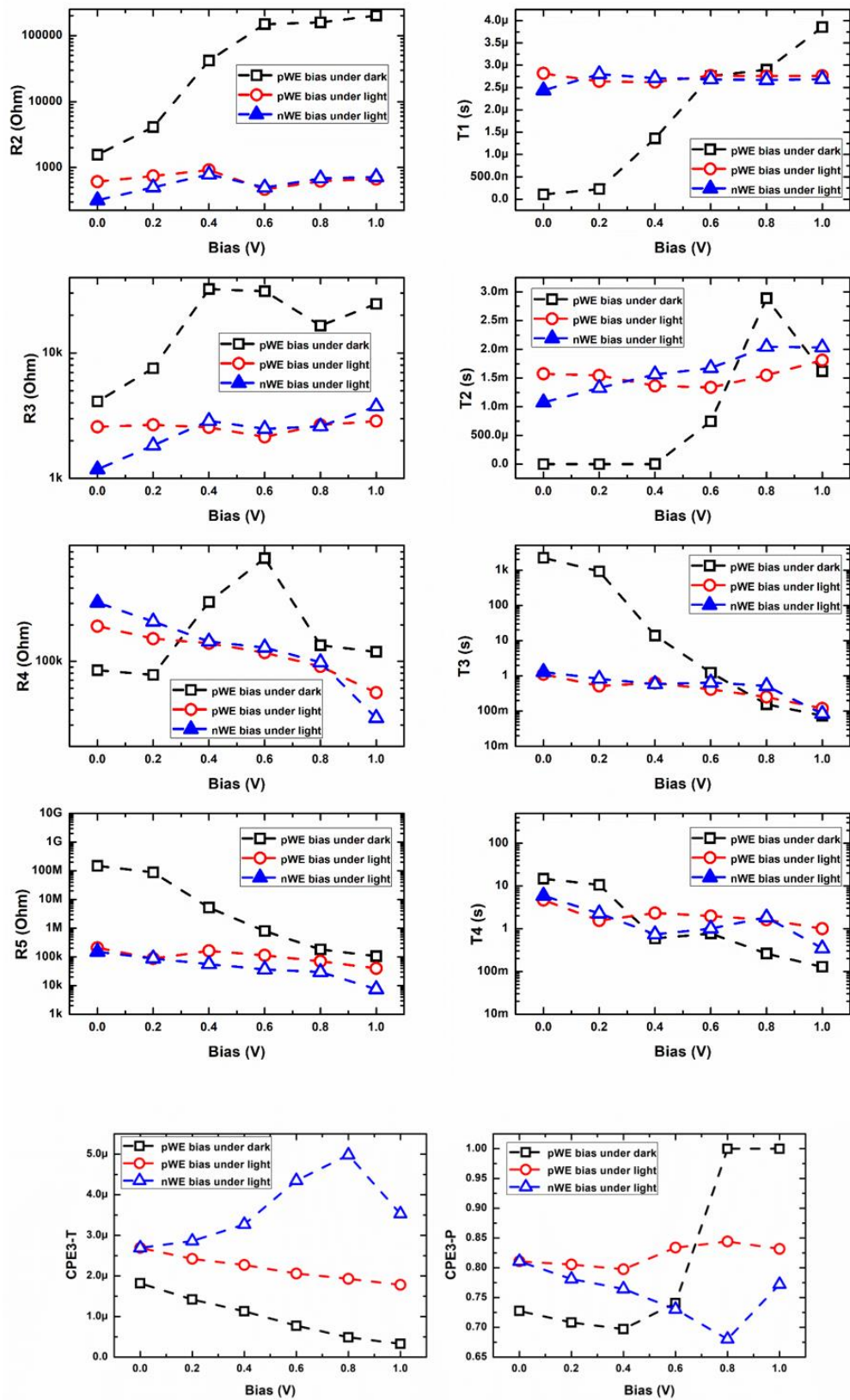


**Figure S1.** Voltage dependence of various fitting parameters (R2, R3, R4, R5, T1, T2, T3, T4, CPE3-T and CPE3-P) obtained from zView simulation of the EIS data using the aforementioned model. (Solid point is extrapolated from the simulated data. Hollow points are simulated data.)

R2 is the  $R_{\text{transport}}$  which arises due to the motion of ions in the bulk. T1 is corresponding time constant associated with R2 and C1 in the perovskite bulk. R3 is  $R_{\text{transfer}}$  originated from the charge transfer across the perovskite-electrolyte interface. T2 is the corresponding time constant associated with R3 and C2 in the depletion region. R4 is the  $R_{\text{liquid}}$  which represents the resistance due to the motion of ions in the liquid electrolyte. T3 is the corresponding time constant associated with R4 and C3 in the Gouy-Chapmann region. R5 is the  $R_{\text{redox}}$  arising from the oxidation and reduction reaction taking place at the perovskite liquid electrolyte interface. T4 is the corresponding time constant associated with R5 and C4 in the Helmholtz region.

R2 is high-frequency resistance with T1 of the order of micro-seconds ( $\mu\text{s}$ ). R3 is mid-frequency resistance with T2 in the range of milli-second (ms). R4 is low frequency resistance with T3 of the order of seconds. R5 is very low-frequency resistance with T4 of tens of second. The monotonic increase in the high-frequency resistance R2 in dark indicates the absence of electron-ion coupling responsible for enhancement of the ionic and electronic conductivity of the perovskite material on illumination.<sup>1</sup> The irregularity in this monotonic behaviour under dark at higher applied bias can be attributed to the contribution from the ions present in the liquid-electrolyte side which start to migrate more at higher applied bias. However, the presence of this electron-ion interaction under light is responsible for the non-monotonic and anomalous behaviour of R2 with applied bias.

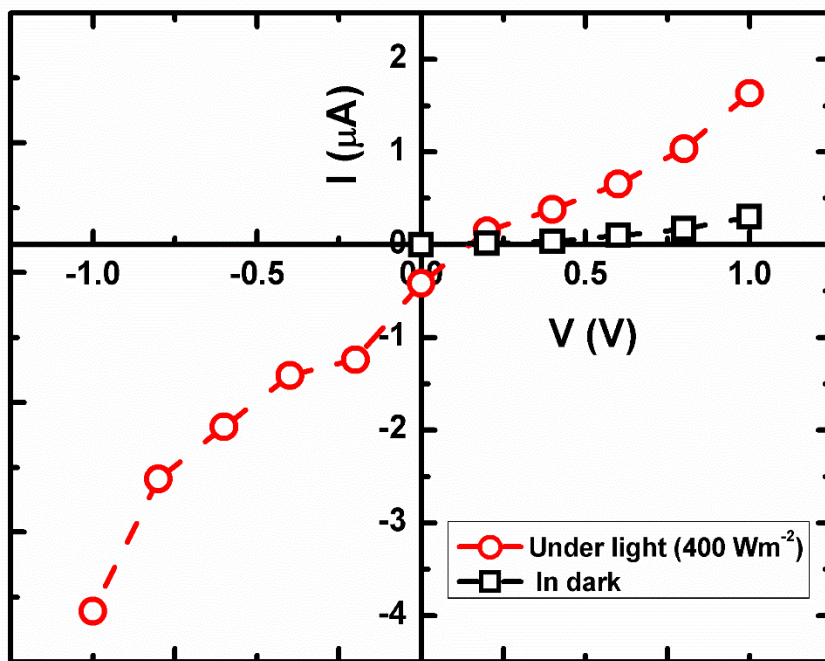


**Figure S2.** Static IV of the ITO|MAPI|liquid-electrolyte|Pt under light ( $400 \text{ Wm}^{-2}$ ) and dark.

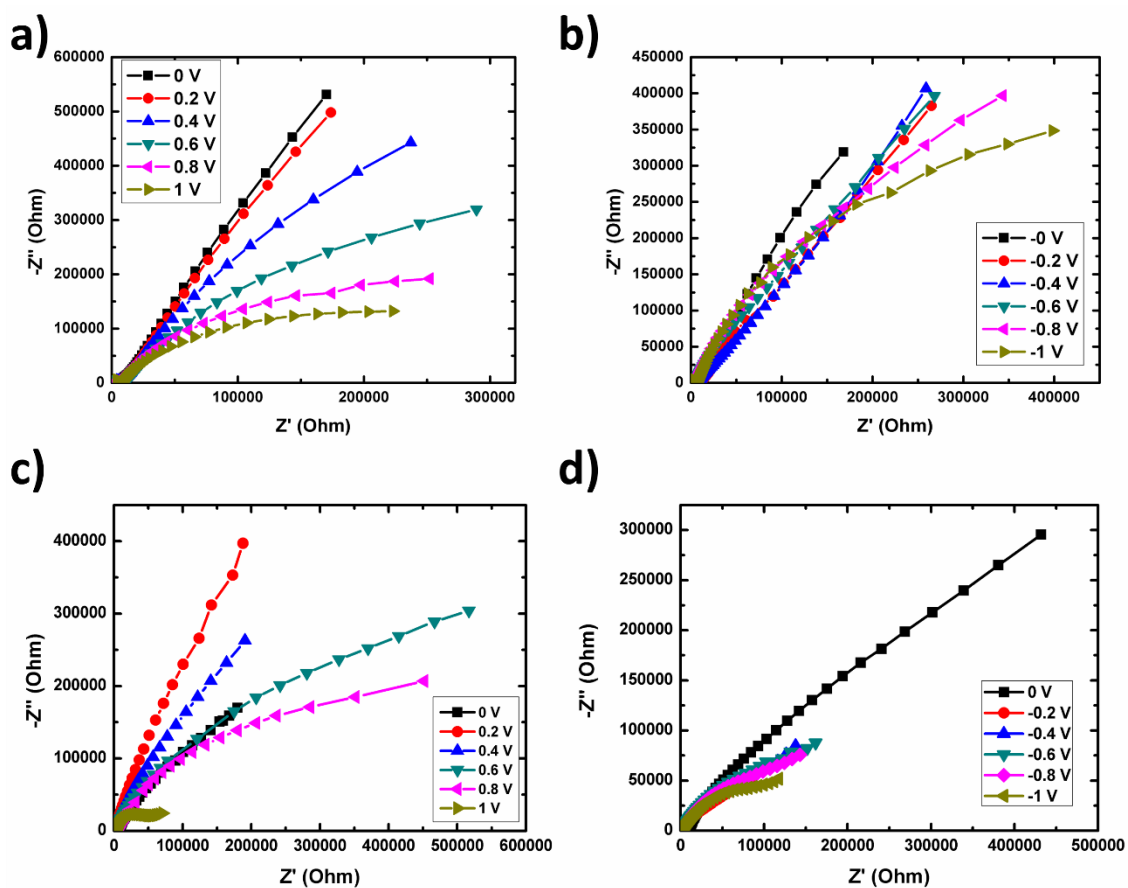


**Figure S3.** Nyquist plot of ITO|P3HT|liquid-electrolyte|Pt under light ( $400\text{Wm}^{-2}$ ) in (a) pWE condition, (b) nWE condition and ITO|PEDOT:PSS|MAPI|liquid-electrolyte|Pt under light ( $400\text{Wm}^{-2}$ ) in (c) pWE condition, (d) nWE condition. Both the devices show voltage dependence EIS feature in pWE condition and voltage independent characteristic in nWE condition.

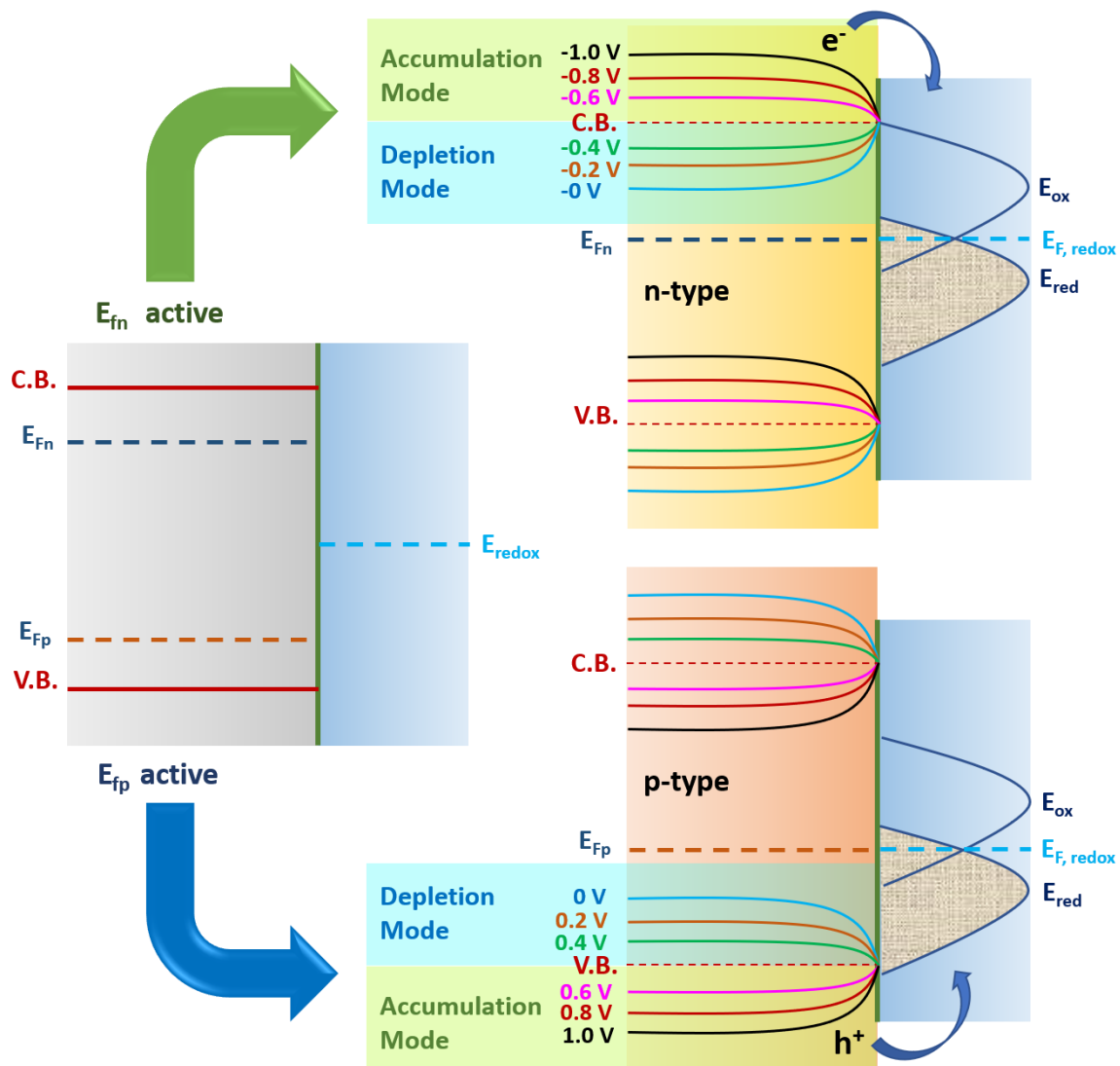


**Figure S4.** Energy band diagram showing depletion and accumulation mode in both nWE and pWE conditions on applying external bias.

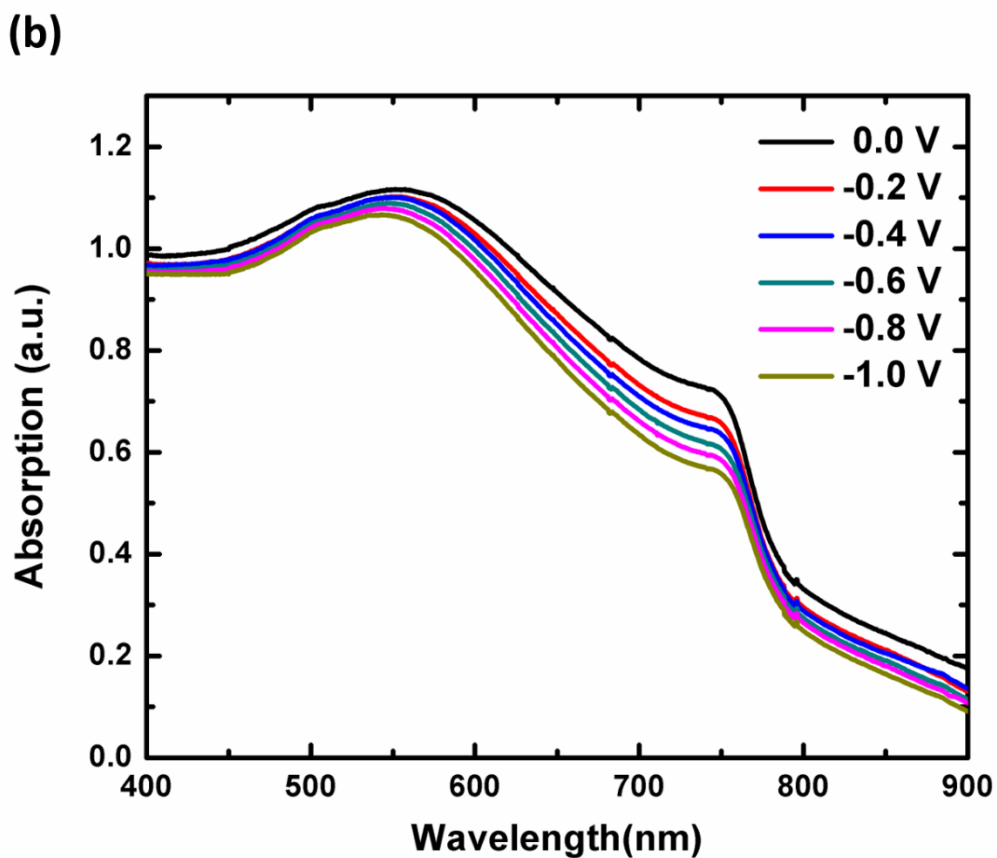
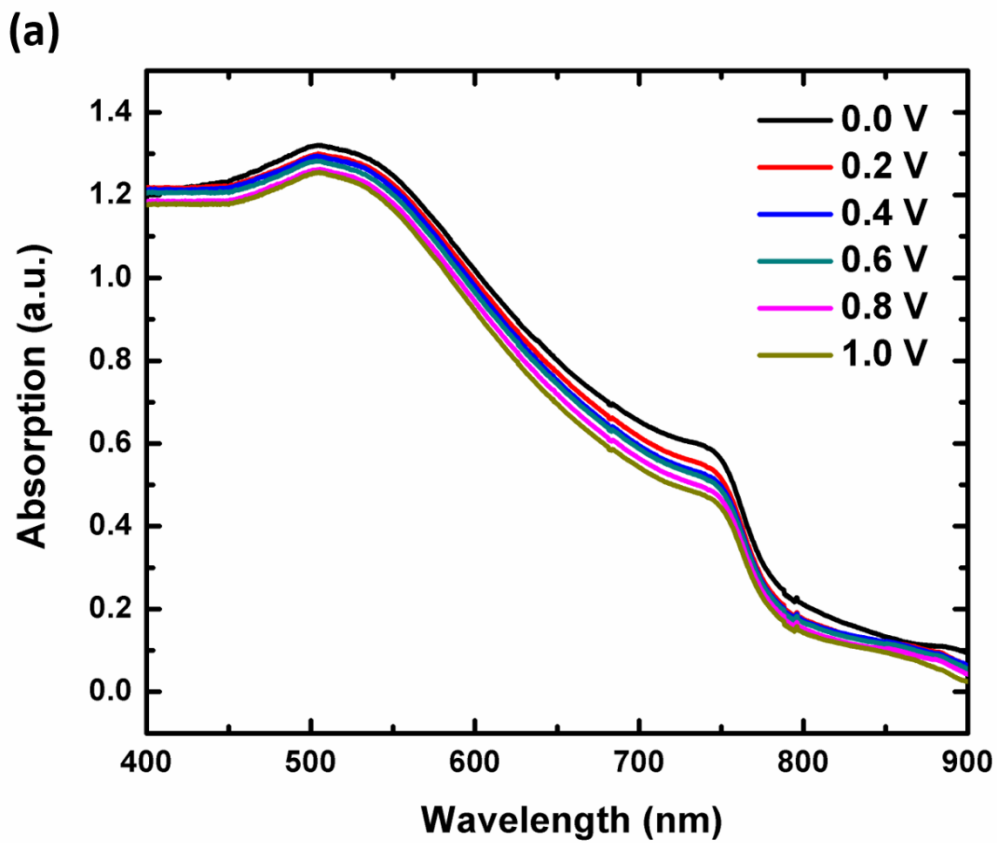


**Figure S5.** UV-Visible absorption spectrum of the device ITO|MAPI|liquid-electrolyte|Pt in both (a) pWE and (b) nWE conditions. The schematic of the experimental setup used for this measurement is shown in Figure S10. The measurements are calibrated.

In order to verify that the reduction in absorption with increase in applied bias shown above is not due to the degradation of perovskite film by liquid electrolyte, we took the absorption spectrum of the device back to back without changing the applied bias. We observed that there was no change in absorption of the device. This shows that the reduction in absorption is not due to the degradation of the film but due to the applied bias. This is shown in the Figure S6 below.

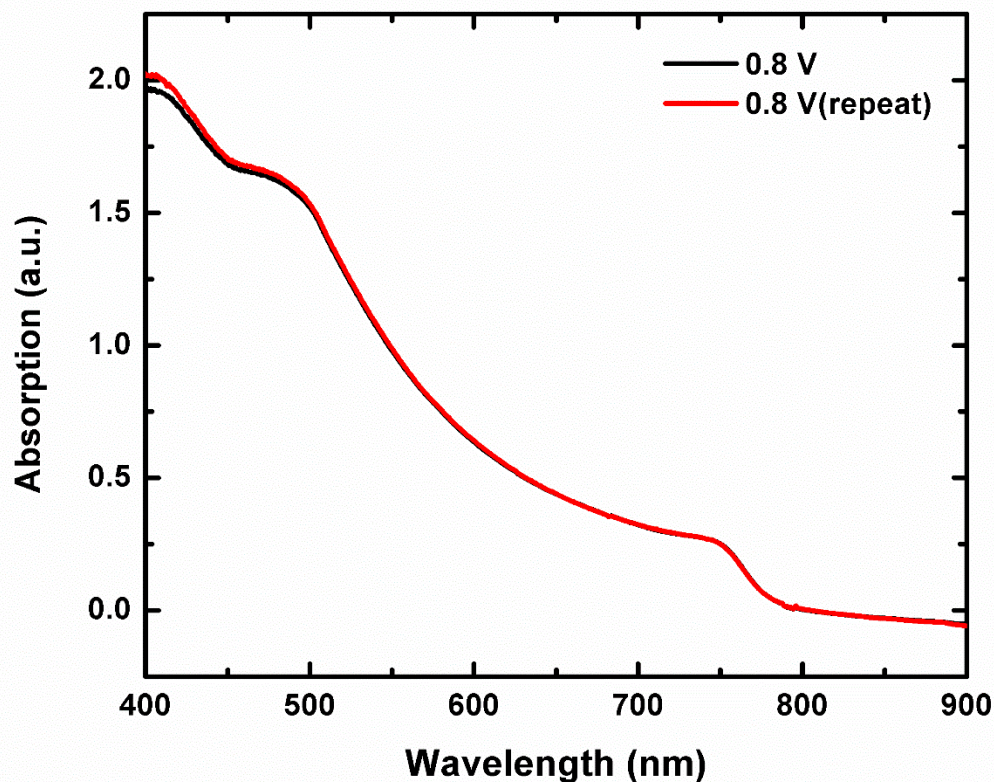


**Figure S6.** The UV-Visible absorption of the same device measured just one after another without changing the applied bias.

The wavelength-dependent reduction in UV-Visible absorption with increase in applied bias as shown in Figure 7 (main text) indicates that this reduction is not due to the degradation of the perovskite film. The degradation of the film will lead to same magnitude of reduction in absorption which would be independent of incident wavelength.



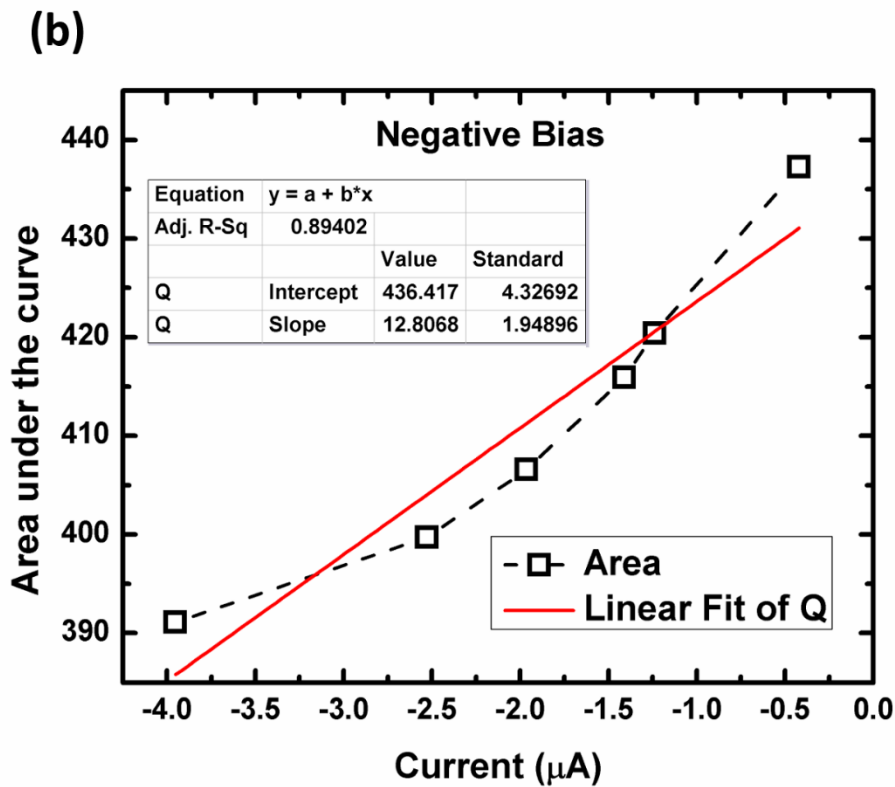
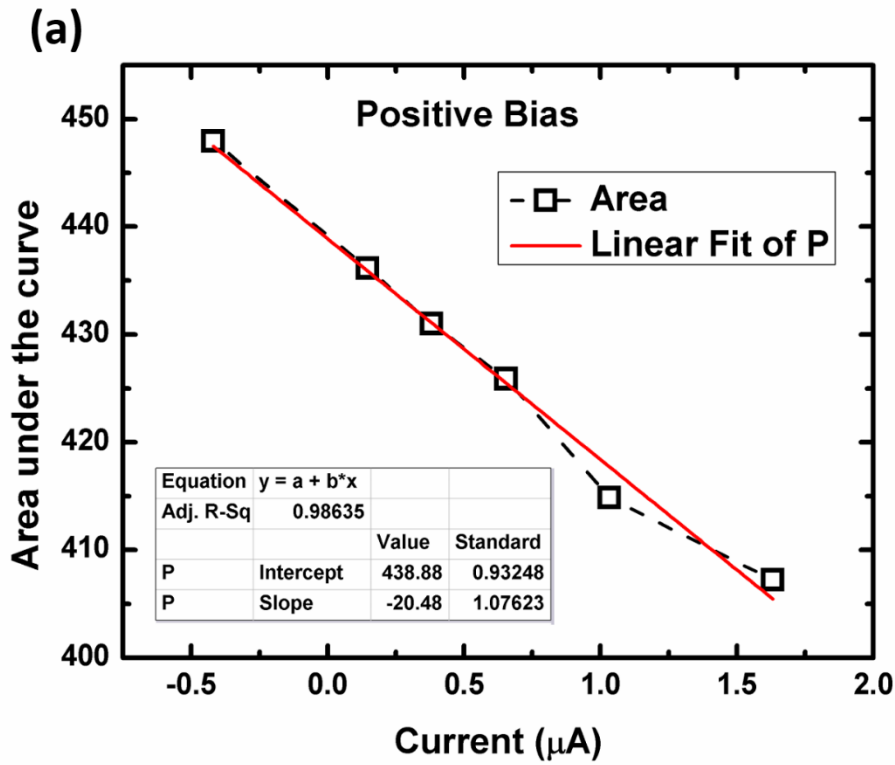


**Figure S7.** Variation of current for the corresponding applied bias with area under the UV-Visible spectra.

The area under the curve was calculated for the complete range of wavelength from 400 nm to 900 nm. The corresponding current is the static current measured across the device at different applied bias. In both the conditions, it can be seen that with increase in bias, the current is increasing and the area under the curve is decreasing.

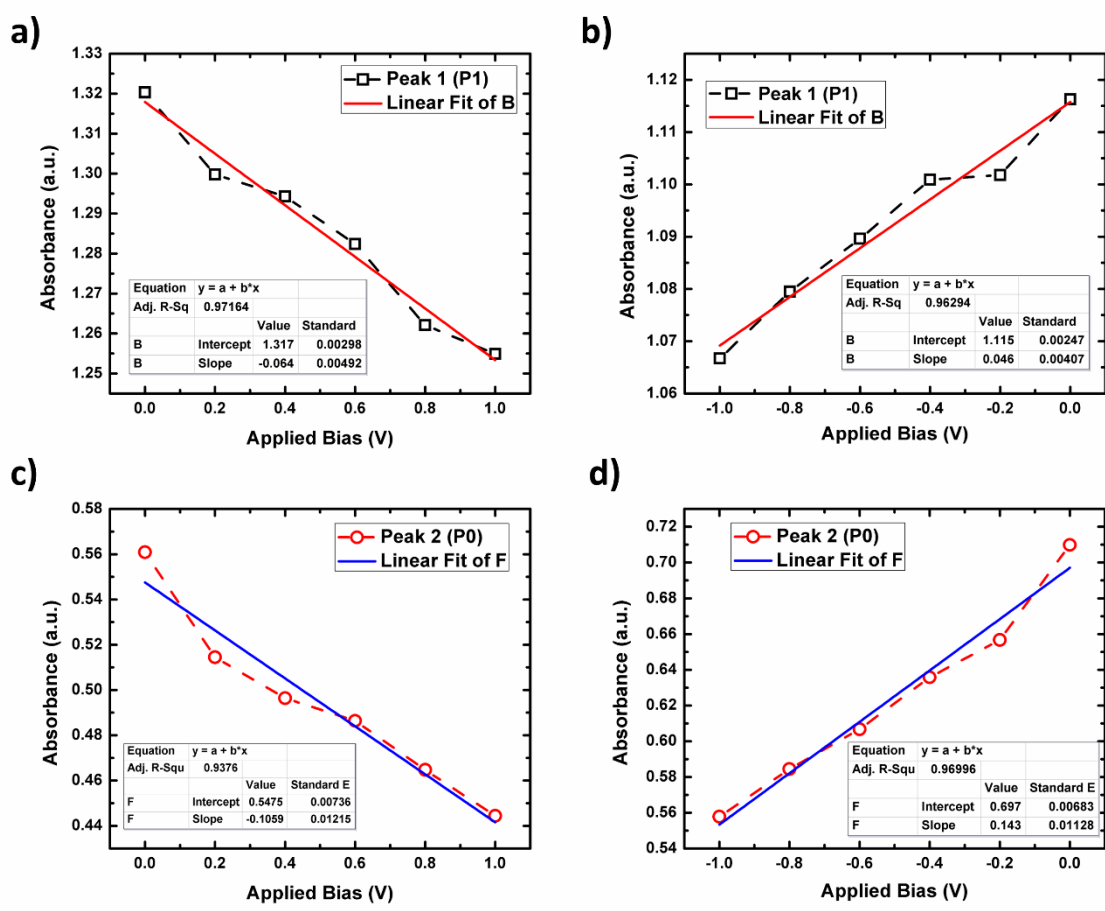


**Figure S8.** Variation of P1 and P0 as a function of applied bias in both pWE (a & c) and nWE (b & d) conditions respectively.

P0 is the absorption at 750 nm wavelength in both nWE and pWE conditions. P1 is the absorption at 504 nm in pWE and around 550 nm in nWE condition. It can be seen that the slope of P0 with bias is around 2-3 times higher than that of P1. This shows that change in P0 is more than the change in P1 with change in applied bias. This means that the absorption is decreasing more drastically at 750 nm band edge than at 504 nm or 550 nm.

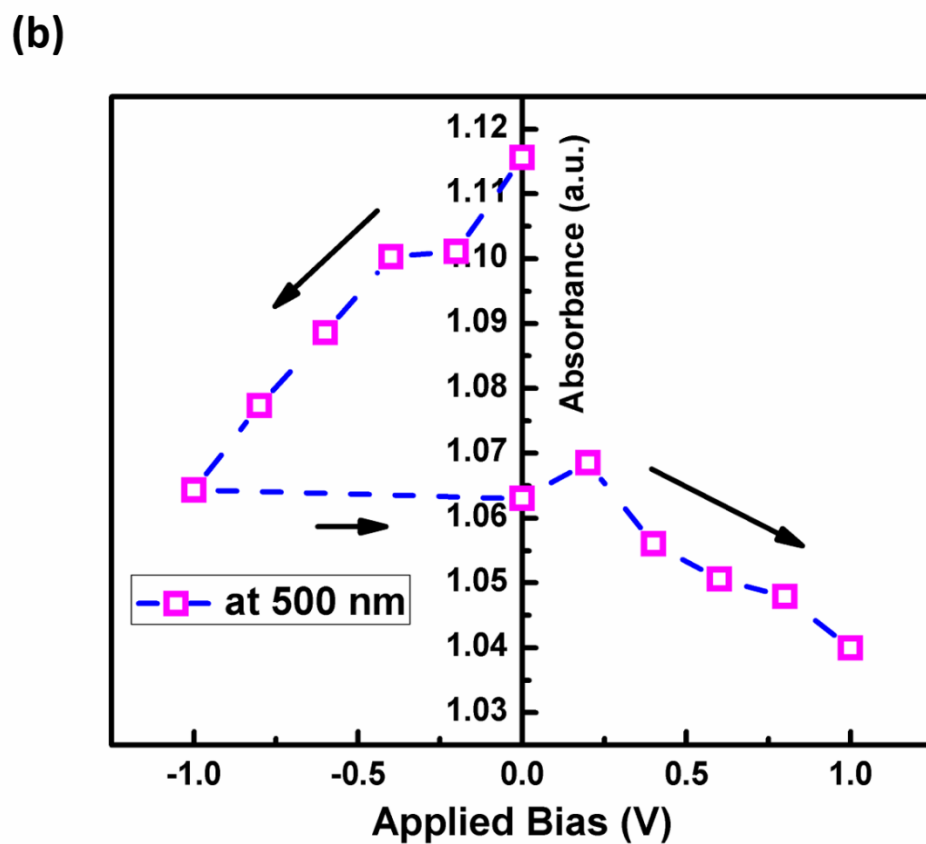
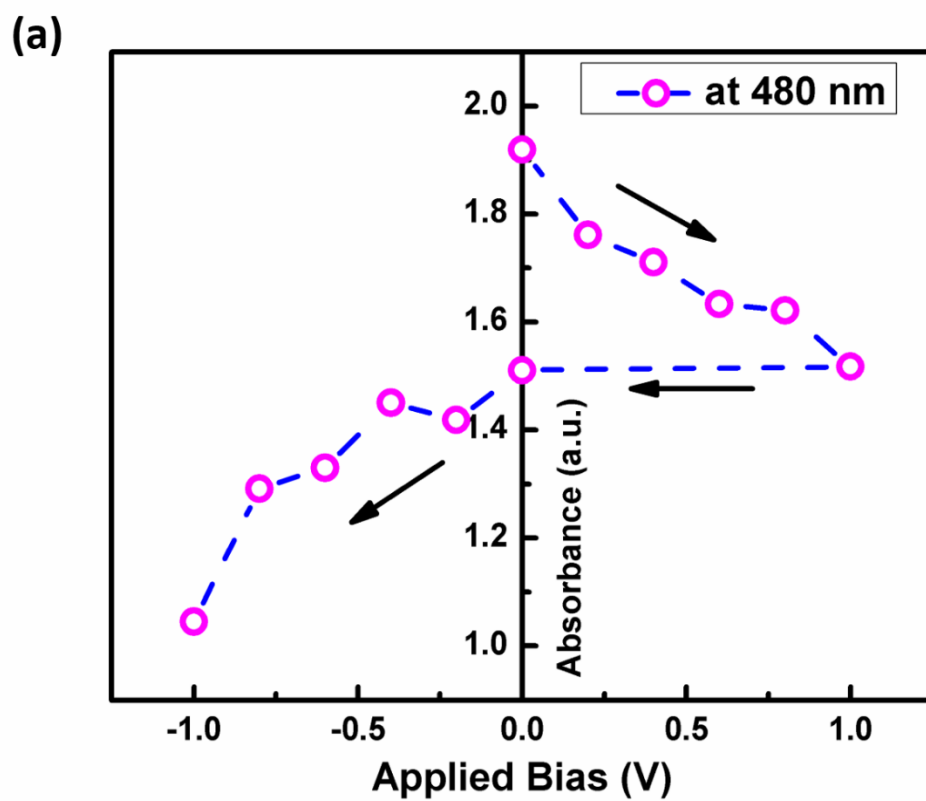


**Figure S9.** Variation of the absorbance with applied bias in cyclic scheme (a) from 0 V to +1 V and then from 0 V to -1 V (pWE first) and (b) from 0 V to -1 V and then from 0 V to +1 V (nWE first).

### Measurement of Bias-dependent UV-Visible Spectroscopy of the perovskite-electrolyte device

The schematic of the experimental setup for the measurement of bias-dependent UV-Visible spectroscopy of the perovskite electrolyte interface is shown in Figure S10. The device ITO|MAPI|liquid-electrolyte|ITO was mounted inside the UV-Visible spectrometer and the dc bias was applied using the potentiostat. The UV-Visible spectrum at different bias is measured just after the other after changing the applied bias. The incident light falls on the counter electrode ITO side first. The measurement was calibrated.

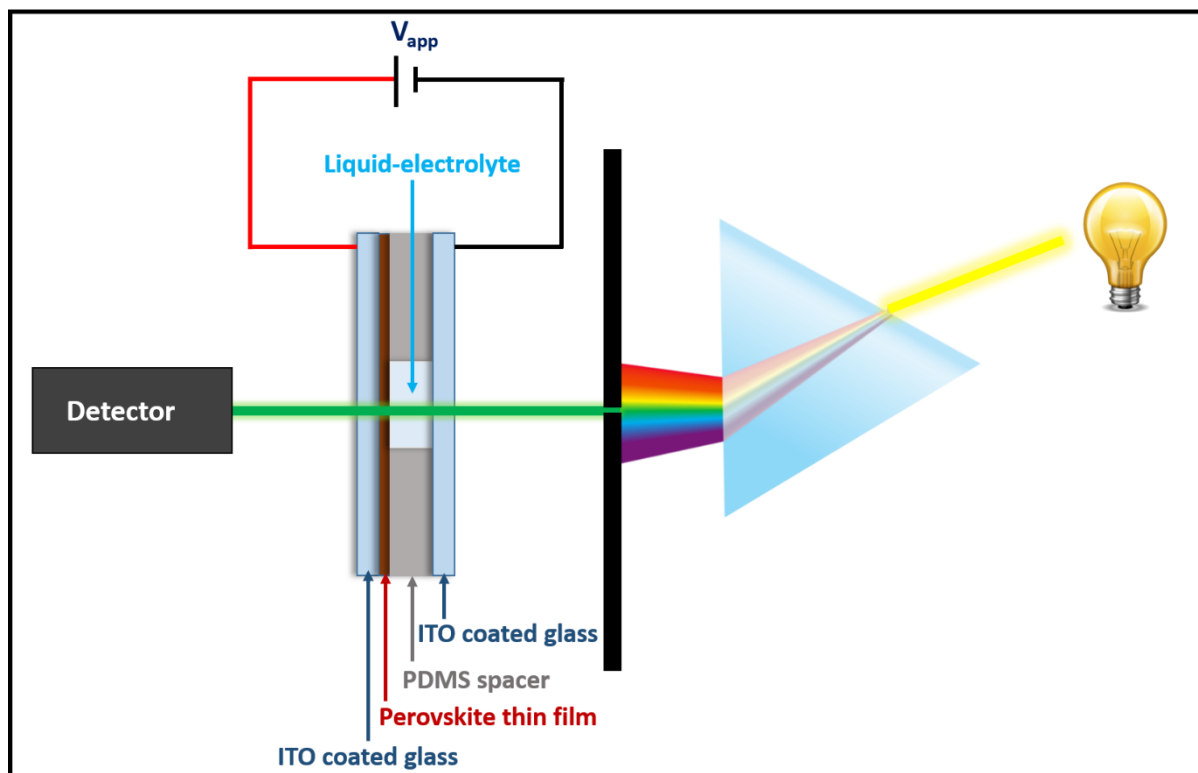


**Figure S10.** Schematic for the measurement of UV-Visible Spectrum of the MAPI-electrolyte device in operation for different applied bias.

### Calculation of $E_{F,redox}$ of liquid electrolyte Tetrabutylammonium hexafluorophosphate (TBAPF<sub>6</sub>) in Dichloromethane (DCM)

The equivalent redox fermi energy ( $E_{F,redox}$ ) of liquid electrolyte was calculated using the formula given below:

$$E_{F,redox} = -(eV_{NHE} + eV_{redox})$$

where  $V_{NHE}$  is the normal hydrogen electrode potential taken as 4.44 V and  $V_{redox}$  is the redox potential of the electrolyte.  $V_{redox}$  of the electrolyte is taken as 0.25 V as measure from cyclic voltammetry.<sup>2</sup> The value of  $E_{F,redox}$  as calculated from above equation of the liquid electrolyte is -4.75 eV.

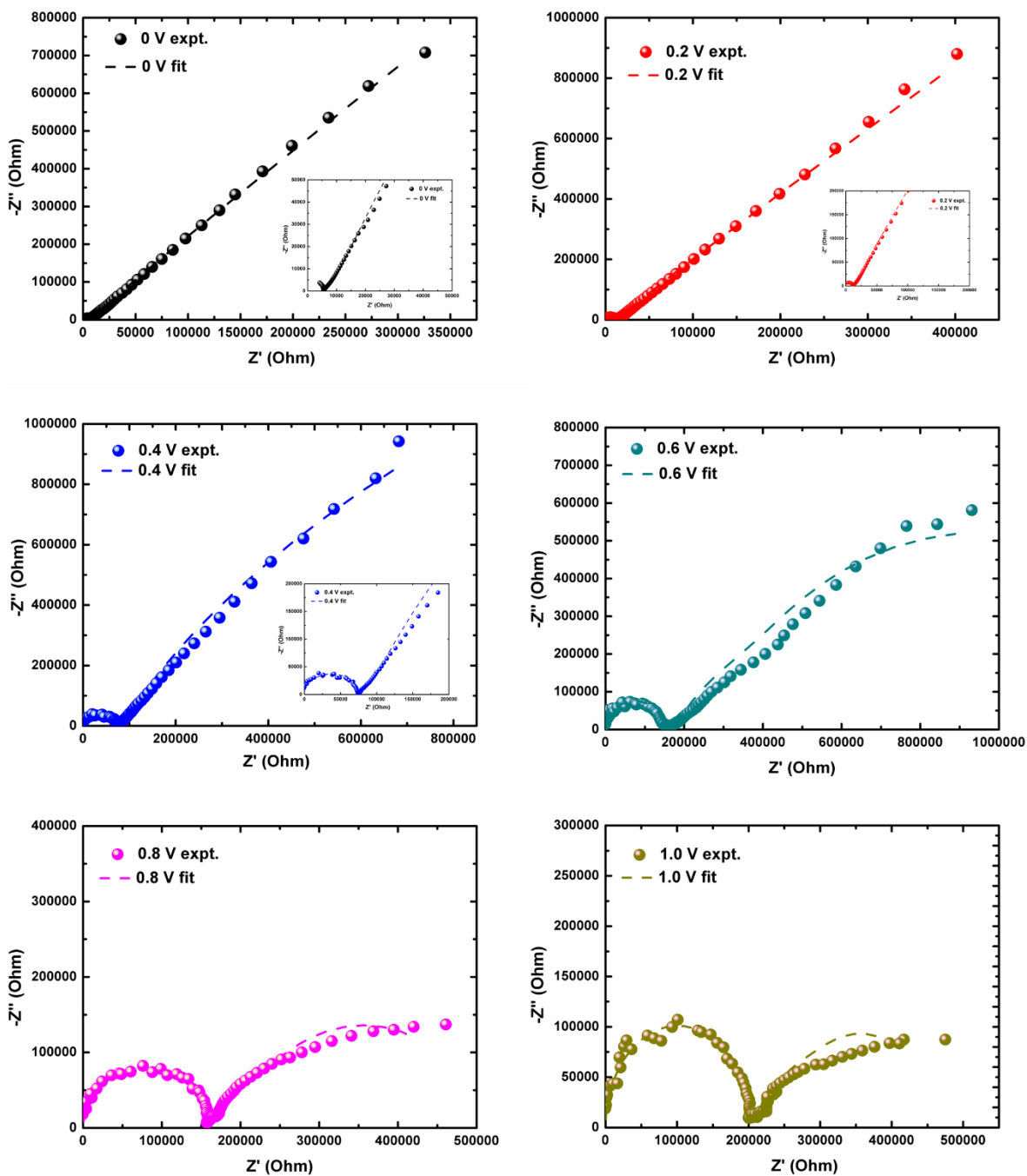


**Figure S11.** Fitting of EIS data of ITO|MAPI|liquid-electrolyte|Pt under dark in pWE condition for different applied bias. The fitting is done in zView software using the model mentioned in main text.

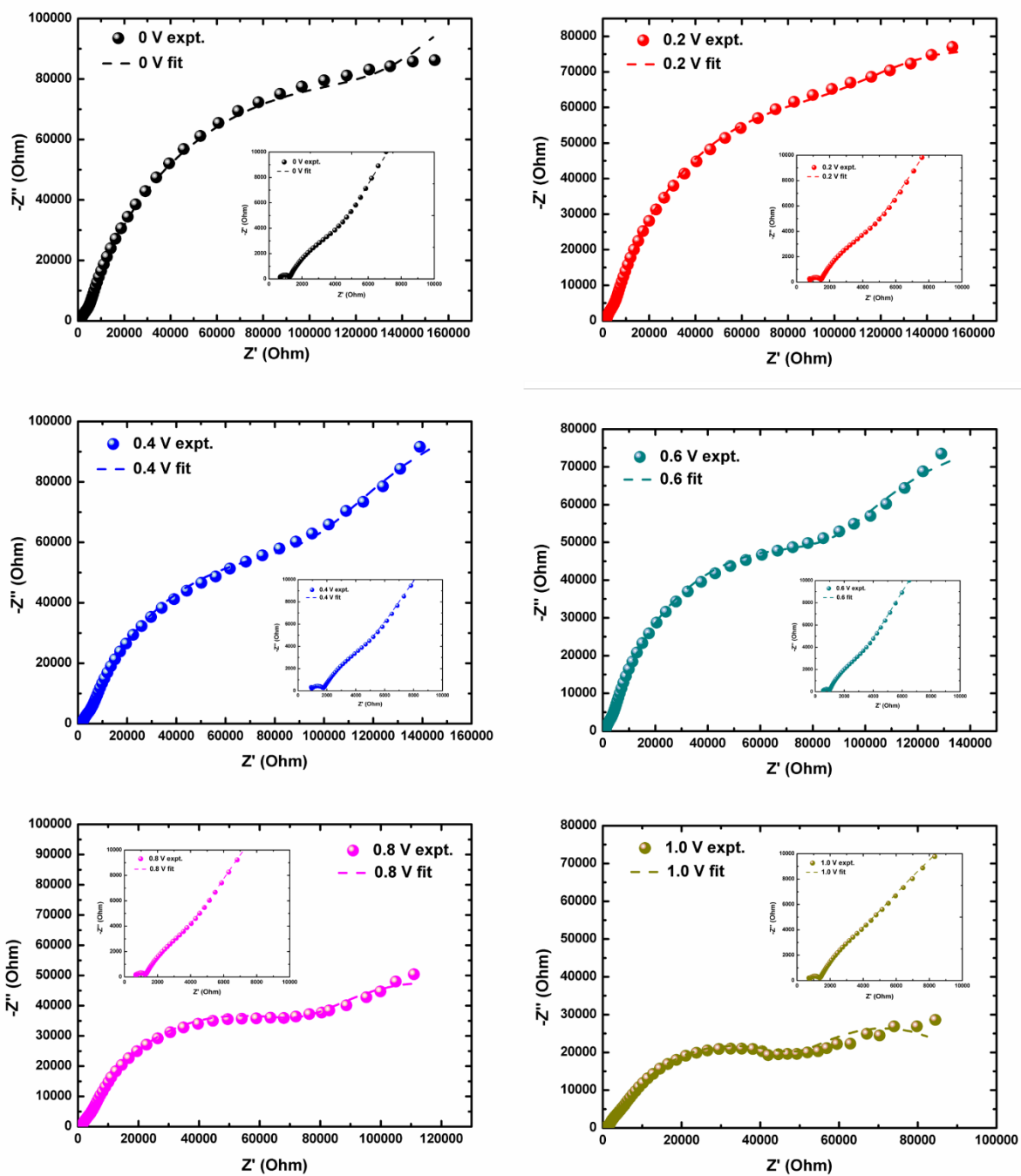


**Figure S12.** Fitting of EIS data of ITO|MAPI|liquid-electrolyte|Pt under light ( $400 \text{ Wm}^{-2}$ ) in pWE condition for different applied bias.

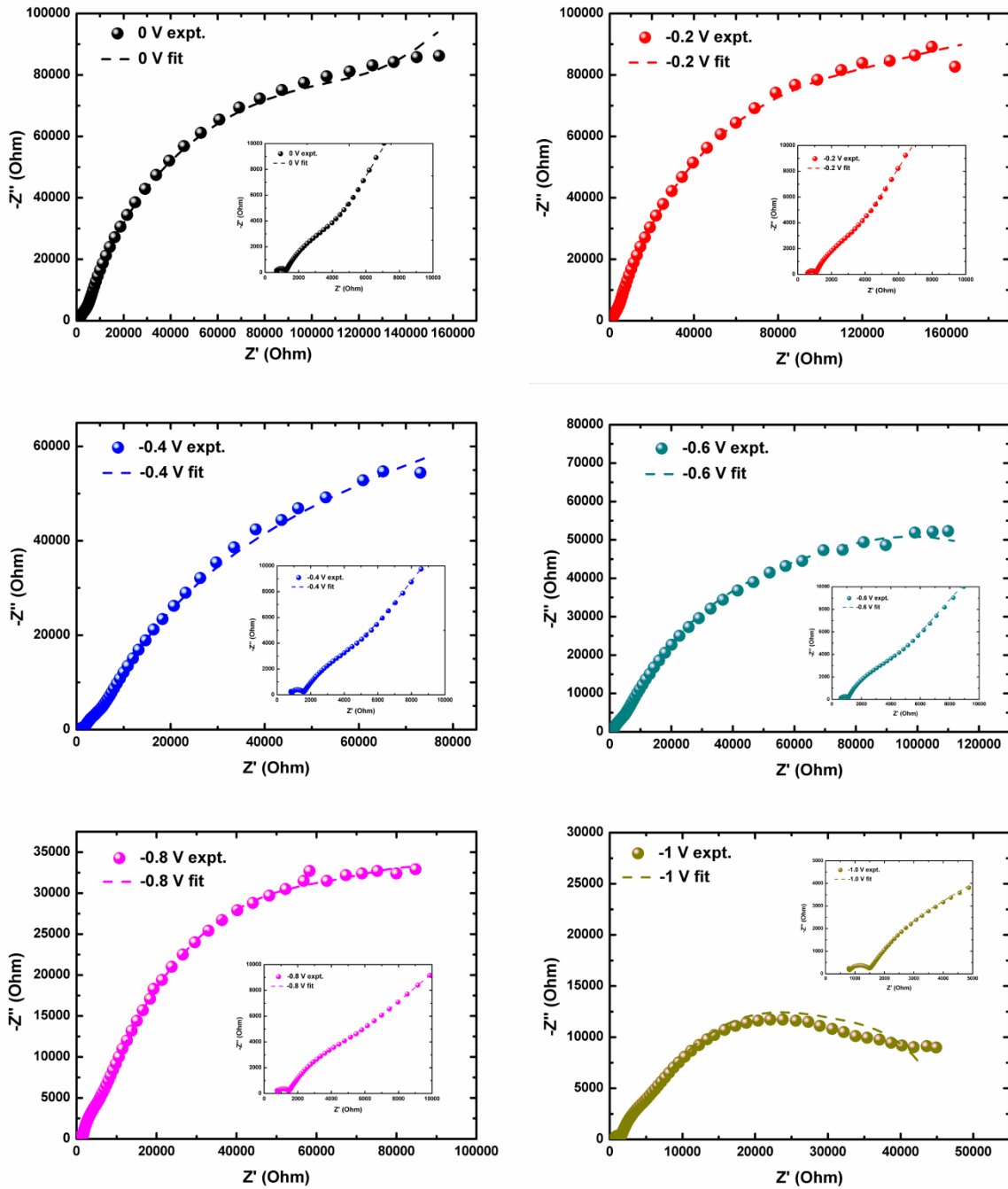


**Figure S13.** Fitting of EIS data of ITO|MAPI|liquid-electrolyte|Pt under light ( $400 \text{ Wm}^{-2}$ ) in nWE condition for different applied bias.

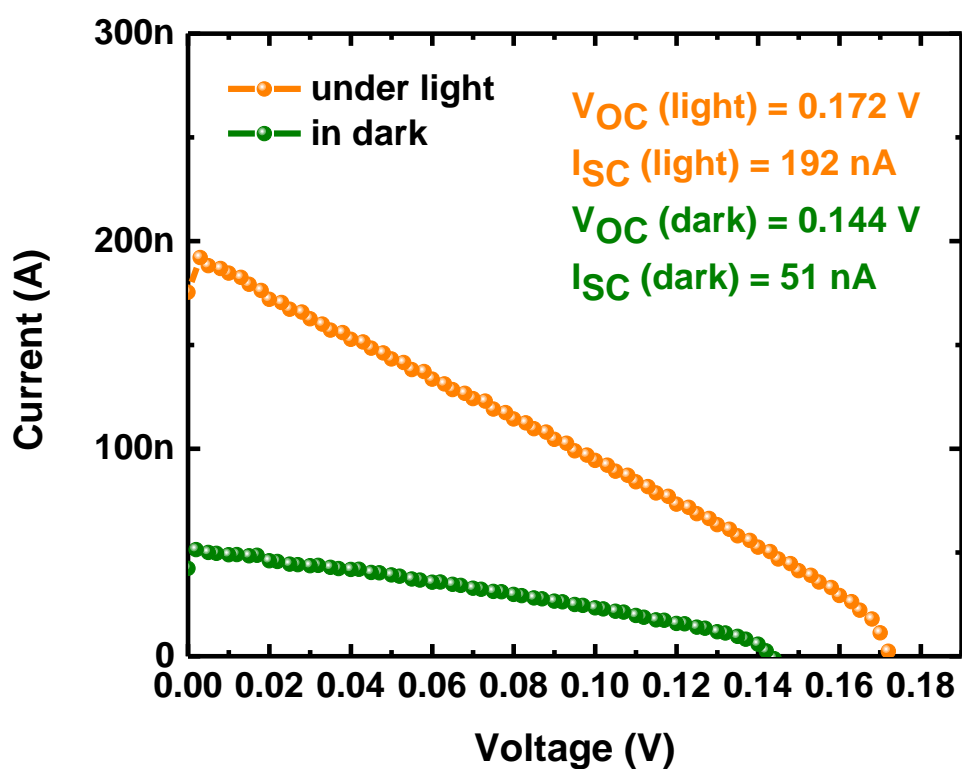


**Figure S14.** IV characteristic of ITO|MAPI|liquid-electrolyte|Pt device under dark and illumination ( $400\text{Wm}^{-2}$ ). The as-prepared devices with MAPI films have  $V_{OC}$  of 0.172 and 0.144 under light and dark, respectively, despite the work functions of ITO and the liquid electrolyte (0.1 M TBAPF6 in DCM) being almost same around -4.75 eV. This might be attributed to the different interfacial electronic and ionic structures at the MAPI|ITO and MAPI|electrolyte contacts.



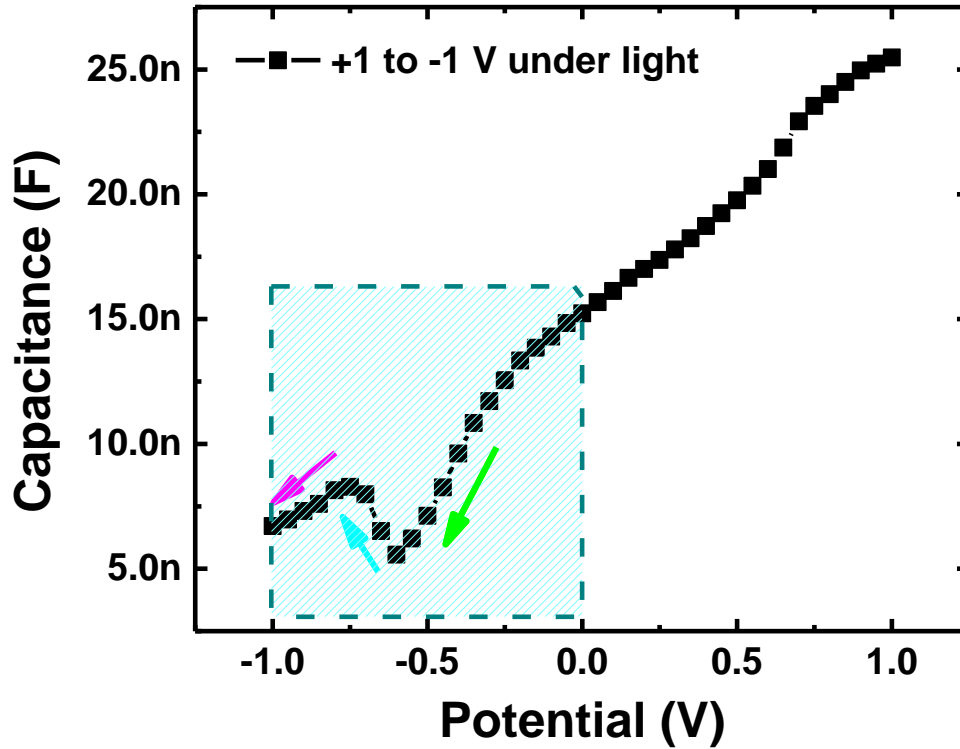


**Figure S15.** Capacitance vs. voltage curve for the device ITO|MAPI|liquid-electrolyte|Pt under light ( $400 \text{ Wm}^{-2}$ ) in the sweep direction from +1 V to -1 V. The magnitude and trend of this capacitance in the blue shaded area is similar to that of  $C_1$  or  $C_{\text{bulk}}$  (high-frequency capacitance) simulated by zView. The capacitance here first decreases with increase in bias (green arrow), then increases (blue arrow) and then again decreases (pink arrow). This trend is similar to that of  $C_1$  shown in Figure 4 (main text). However, there is a shift in the changing point which might be attributed to the hysteresis due initially applied positive bias. The regions denoted by green, blue and pink arrow corresponds to the three regions observed in  $-Z''$  vs. frequency plot (Figure 1 of main text).

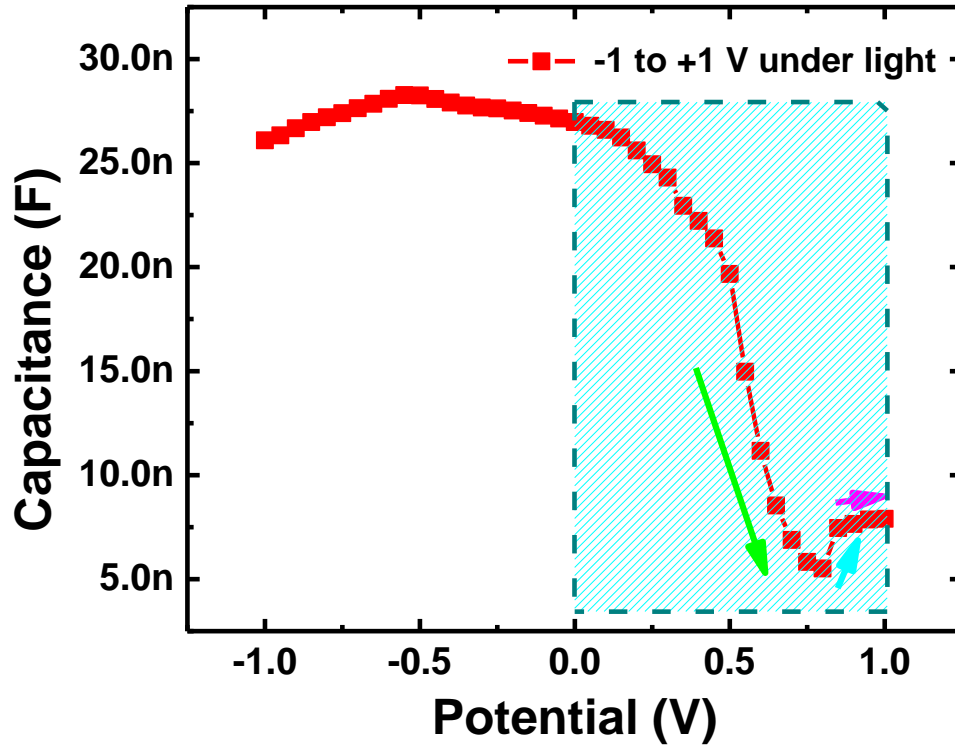


**Figure S16.** Capacitance vs. voltage curve for the device ITO|MAPI|liquid-electrolyte|Pt under light in the sweep direction from -1 V to +1 V. The magnitude and trend of this capacitance in the blue shaded area is similar to that of  $C_1$  or  $C_{\text{bulk}}$  (high-frequency capacitance) simulated by zView. The capacitance here first decreases with increase in bias (green arrow), then increases (blue arrow) and then saturates (pink arrow). This trend is similar to that of  $C_1$  as shown in Figure 4 (main text). However, there is a shift in the changing point which might be attributed to the hysteresis due initially applied positive bias. The regions denoted by green, blue and pink arrow corresponds to the three regions observed in  $-Z''$  vs. frequency plot (Figure 1 of main text).

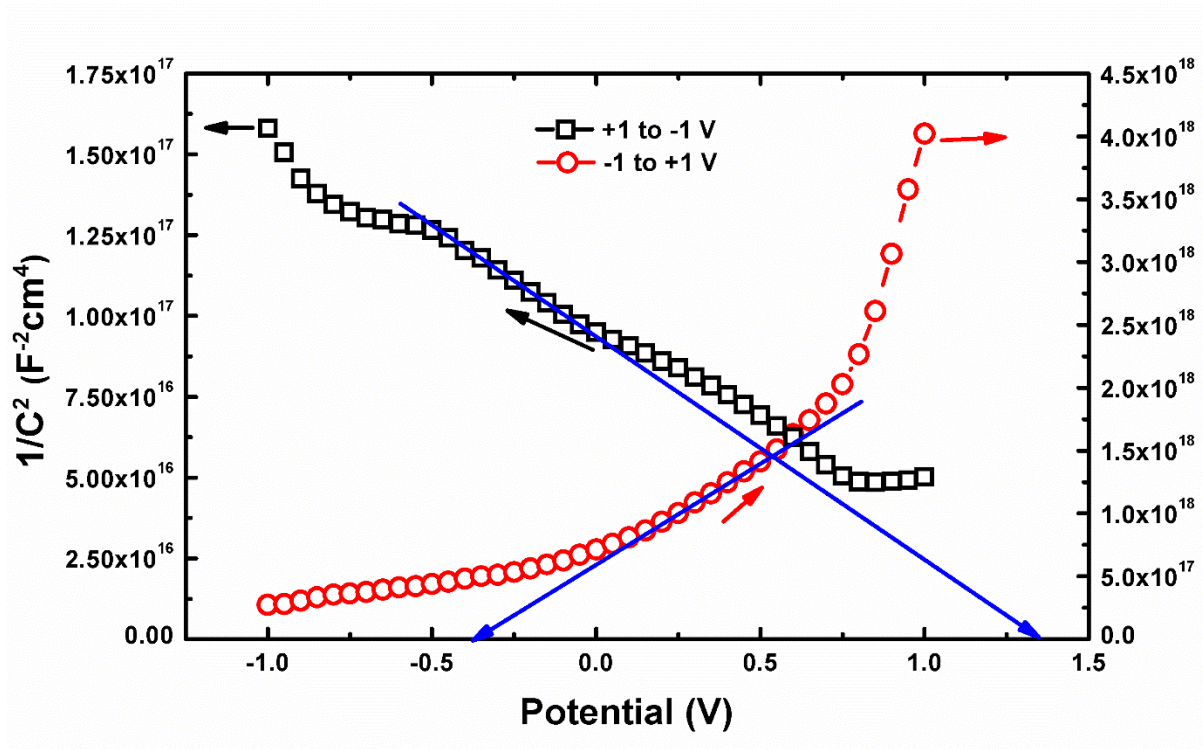


**Figure S17.** Mott-Schottky plot of the ITO|MAPI|liquid-electrolyte|Pt in dark in both directions (+1 V to -1 V and -1 V to +1 V).

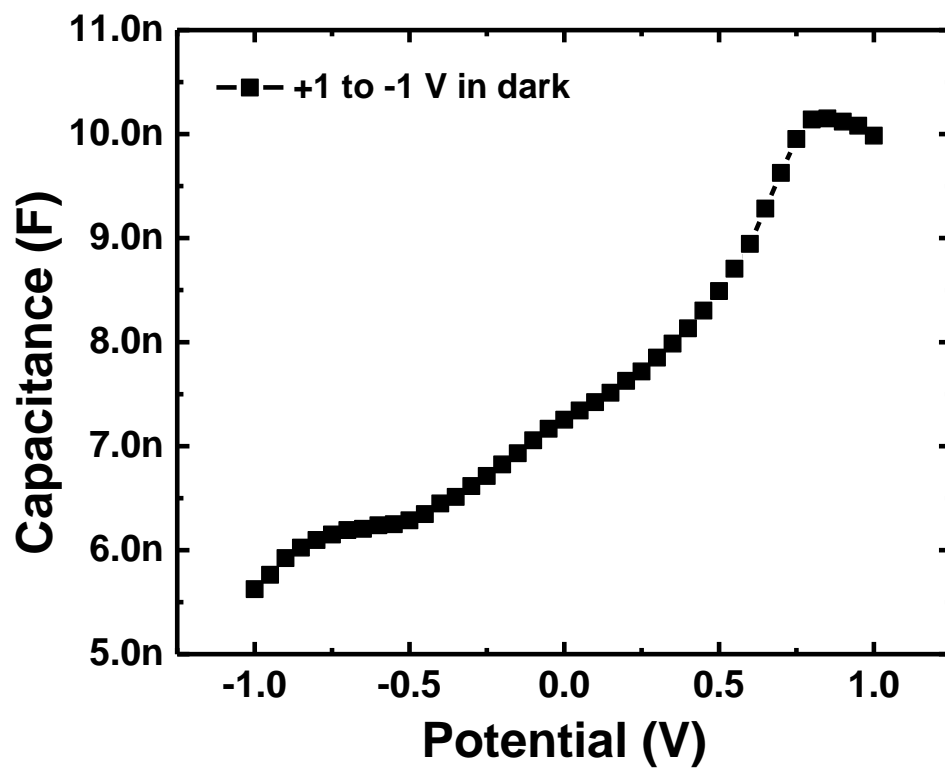


**Figure S18.** Capacitance vs. voltage curve for the device ITO|MAPI|liquid-electrolyte|Pt in dark in the sweep direction from +1 V to -1 V.

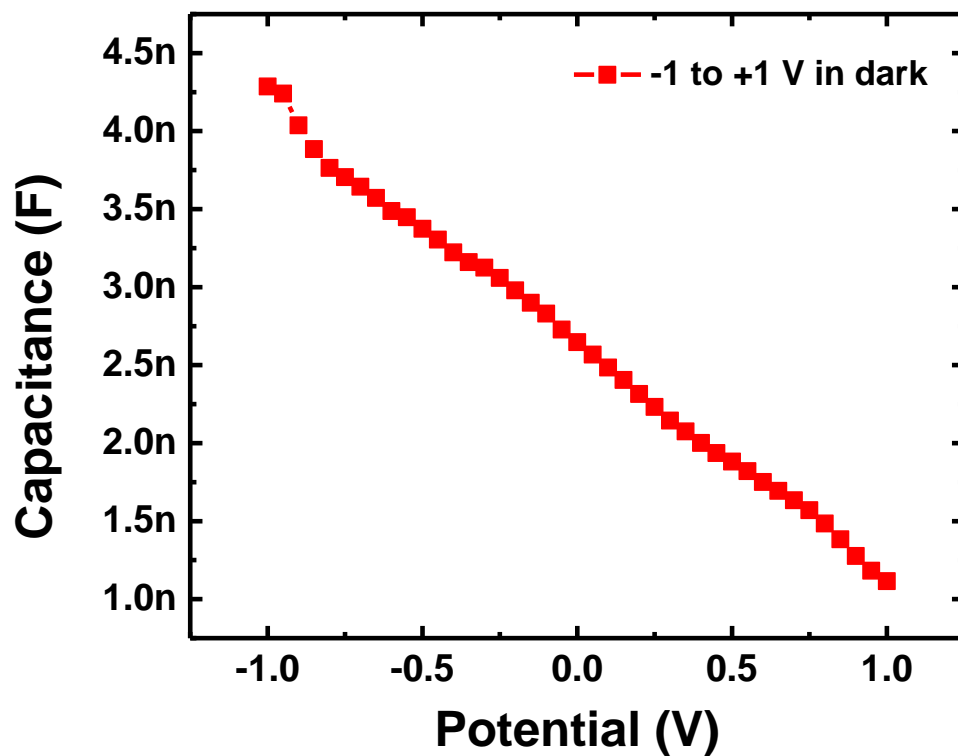


**Figure S19.** Capacitance vs. voltage curve for the device ITO|MAPI|liquid-electrolyte|Pt in dark in the sweep direction from -1 V to +1 V. The capacitance here is monotonically decreasing with increase in applied bias (from 0 V to +1 V) which is same as the simulated capacitance as shown in Figure 1 (main text).

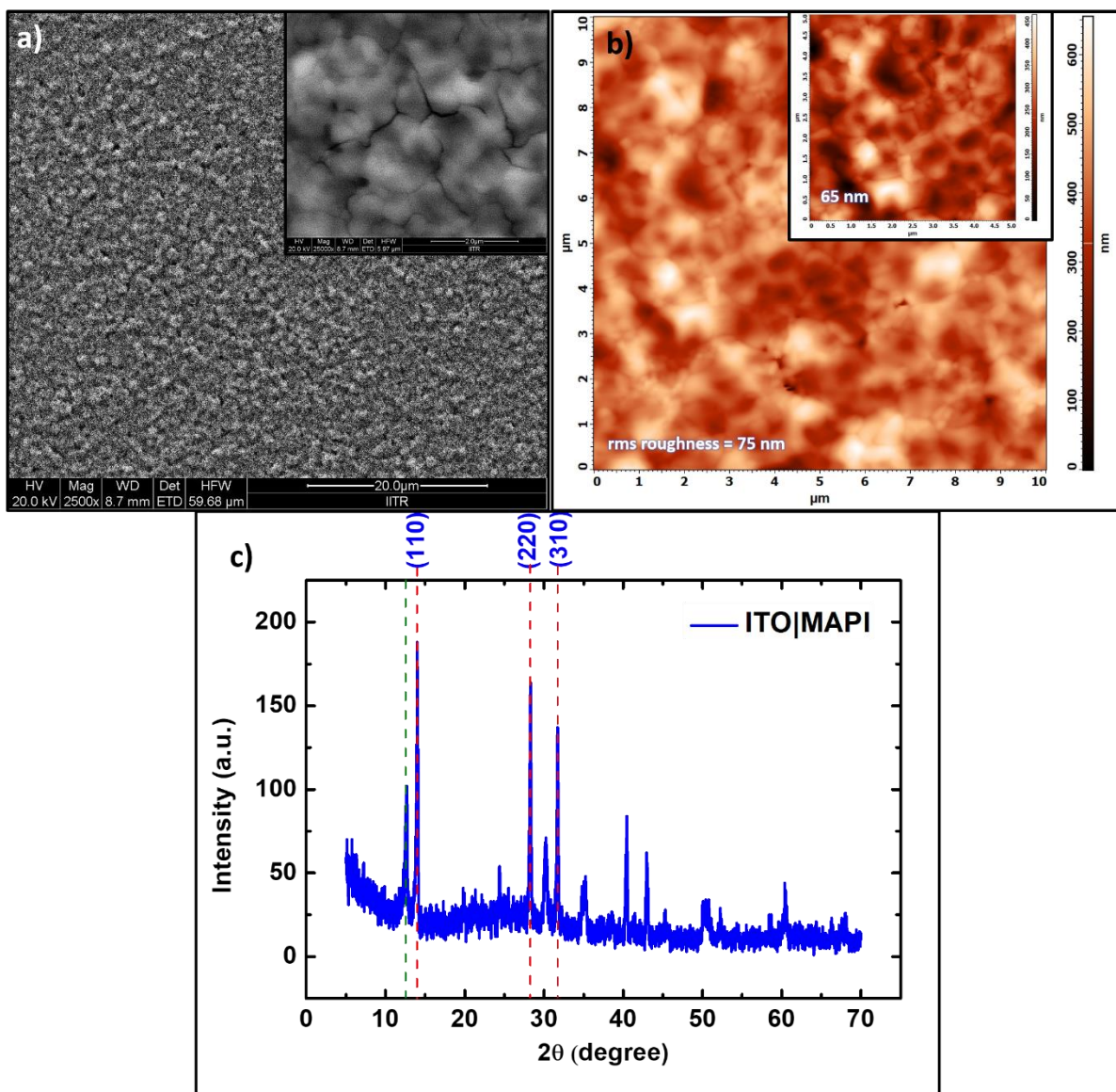


**Figure S20.** (a) Top view FE-SEM images of ITO|MAPI film. The magnification of FE-SEM images is 2500X (main) and 25000X (inset). (b) AFM images of ITO|MAPI film. The rms roughness of the films calculated from AFM is 75 nm (for scan area of 10  $\mu\text{m}$  X 10  $\mu\text{m}$ ) and 65 nm (for scan area of 5  $\mu\text{m}$  X 5  $\mu\text{m}$ ). (c) Thin-film XRD of ITO|MAPI film. Peaks indicated by red dotted lines ( $\sim 14^\circ$ ,  $\sim 28.5^\circ$ , and  $\sim 32^\circ$ ) correspond to the characteristic MAPI peak. Peak indicated by the green dotted line ( $\sim 12.6^\circ$ ) corresponds to the lead iodide peak. Structural characterizations of perovskite polycrystalline thin films were done by Field Emission Scanning Electron Microscope (FE-SEM QUANTA 200 FEG), Atomic Force Microscopy (AFM NT-MDT-INTEGRA) and X-ray diffractometer (Bruker XRD D8-Advance) using Cu-Kr = 1.54  $\text{\AA}$  in angle range  $5^\circ$ – $70^\circ$ .

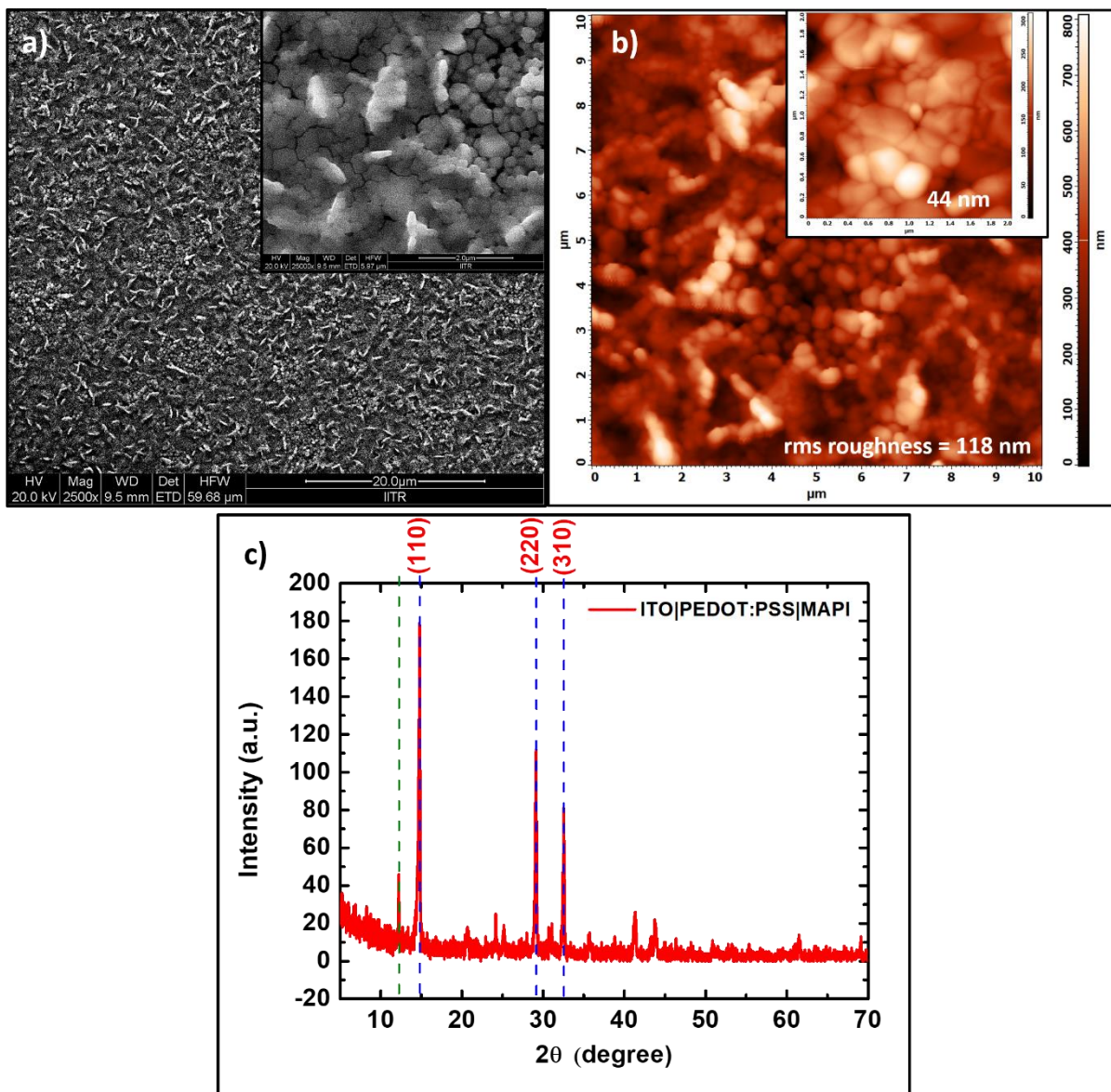


**Figure S21.** (a) Top view FE-SEM images of ITO|PEDOT:PSS|MAPI film. The magnification of FE-SEM images is 2500X (main) and 25000X (inset). (b) AFM images of ITO|PEDOT:PSS|MAPI film. The rms roughness of the films calculated from AFM is 118 nm (for scan area of 10  $\mu\text{m}$  X 10  $\mu\text{m}$ ) and 44 nm (for scan area of 2  $\mu\text{m}$  X 2  $\mu\text{m}$ ). (c) Thin-film XRD of ITO| PEDOT: PSS |MAPI film. Peaks indicated by red dotted lines ( $\sim 14^\circ$ ,  $\sim 28.5^\circ$ , and  $\sim 32^\circ$ ) correspond to the characteristic MAPI peak. Peak indicated by the green dotted line ( $\sim 12.6^\circ$ ) corresponds to the lead iodide peak. Structural characterizations of perovskite polycrystalline thin films were done by Field Emission Scanning Electron Microscope (FE-SEM QUANTA 200 FEG), Atomic Force Microscopy (AFM NT-MDT-INTEGRA) and X-ray diffractometer (Bruker XRD D8-Advance) using Cu-K $\alpha$  = 1.54  $\text{\AA}$  in angle range  $5^\circ$ – $70^\circ$ .

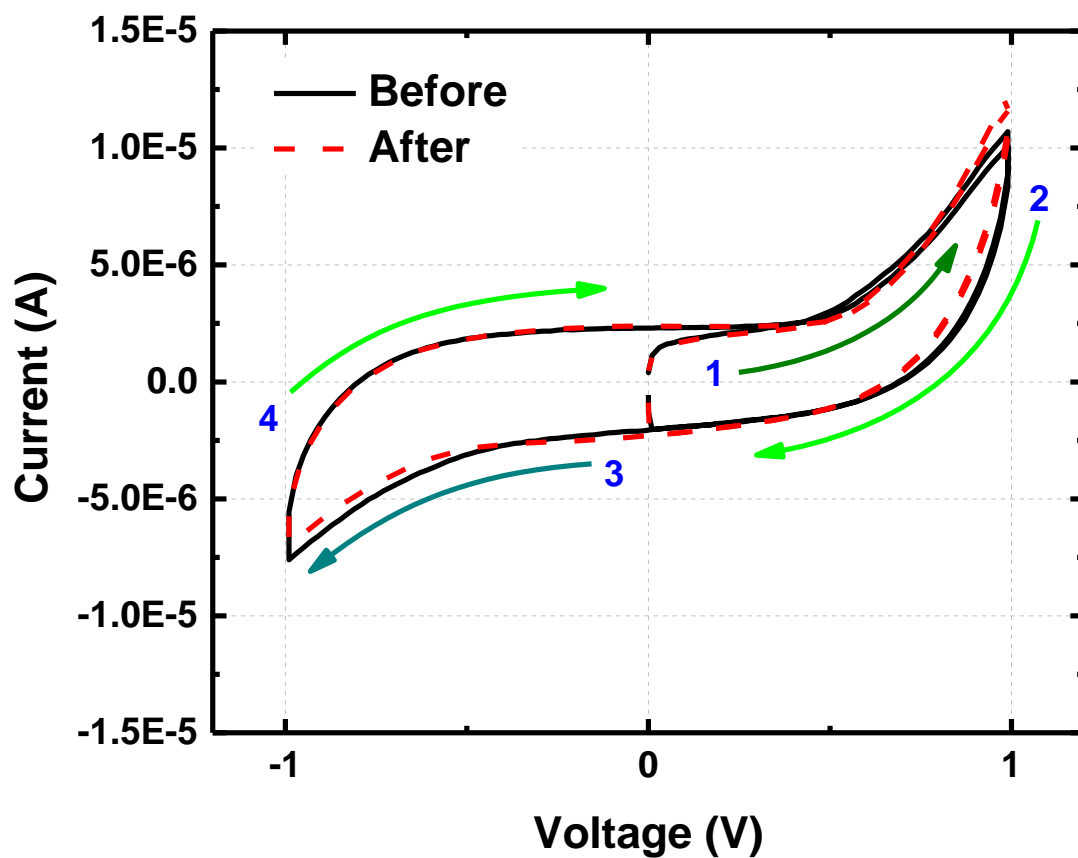


**Figure S22.** Cyclic Voltammetry measurement of the ITO|MAPI|liquid-electrolyte|Pt under light ( $400\text{Wm}^{-2}$ ) before and after impedance measurements. The measurement is done in the direction starting from  $0\text{ V} \rightarrow +1\text{ V} \rightarrow 0\text{ V} \rightarrow -1\text{ V} \rightarrow 0\text{ V} \rightarrow +1\text{ V} \rightarrow 0\text{ V}$ . There are not much of changes in the CV data before and after the EIS measurements indicating not much of degradation/changes at the solid-liquid interface during the measurement.



**Table S1.** Fitting parameters of the equivalent circuits of the EIS plot of the ITO|MAPI|liquid-electrolyte| Pt device under dark at different applied bias (pWE) condition shown in Figure 1a, b.

Applied Bias (V)	R2 $\Omega$	R3 $\Omega$	R4 $\Omega$	R5 $\Omega$	C1 F	C2 F	C3 F	C4 F
0	1563	4111	84651	1.5E8	6.69E-11	2.54E-11	1.48605E-5	9.87E-8
0.2	4106	7551	77653	8.84E7	5.47E-11	2.98E-11	1.04098E-5	1.2E-7
0.4	41870	32356	309000	5.24E6	3.25E-11	4.21E-11	2.50784E-6	1.13E-7
0.6	149030	31124	707000	803000	1.85E-11	2.39E-8	8.18862E-7	9.61E-7
0.8	158460	16502	136000	183000	1.83E-11	1.75E-7	4.89E-7	1.43E-6
1.0	201850	24677	120000	106000	1.91E-11	6.55E-8	3.28E-7	1.21E-6

**Table S2.** Fitting parameters of the equivalent circuits of the EIS plot of the ITO|MAPI|liquid-electrolyte| Pt device under illumination ( $400 \text{ Wm}^{-2}$ ) at different applied bias (pWE) condition shown in Figure 1f, g.

Applied Bias (V)	R2 $\Omega$	R3 $\Omega$	R4 $\Omega$	R5 $\Omega$	C1 F	C2 F	C3 F	C4 F
0	610	2582	195000	208000	4.62E-9	6.09E-7	2.74114E-6	2.25E-5
0.2	747.2	2674	154000	88560	3.53E-9	5.78E-7	2.12794E-6	1.76E-5
0.4	919.7	2553	141000	163000	2.85E-9	5.34E-7	2.06619E-6	1.43E-5
0.6	467.9	2141	118000	114000	5.92E-9	6.24E-7	1.77832E-6	1.74E-5
0.8	622.3	2672	90971	70723	4.43E-9	5.79E-7	1.55675E-6	2.29E-5
1.0	670.5	2867	55275	40250	4.12E-9	6.32E-7	1.24411E-6	2.49E-5

**Table S3.** Fitting parameters of the equivalent circuits of the EIS plot of the ITO|MAPI|liquid-electrolyte| Pt device under illumination ( $400 \text{ Wm}^{-2}$ ) at different applied bias (nWE) condition shown in Figure 1k, l.

Applied Bias (V)	R2 $\Omega$	R3 $\Omega$	R4 $\Omega$	R5 $\Omega$	C1 F	C2 F	C3 F	C4 F
0	320	1182	305000	152000	7.62E-9	9.1E-7	2.82275E-6	3.9E-5
-0.2	501.2	1835	213000	88572	5.59E-9	7.23E-7	2.74383E-6	2.57E-5
-0.4	788.9	2875	146000	56440	3.44E-9	5.44E-7	2.87997E-6	1.31E-5
-0.6	498.8	2488	130000	36679	5.38E-9	6.73E-7	3.86339E-6	2.75E-5
-0.8	686.3	2604	98472	29841	3.89E-9	7.85E-7	4.03472E-6	6.16E-5
-1.0	719.4	3752	34285	7561	3.74E-9	5.42E-7	2.0077E-6	4.58E-5

**Work done in Previous Studies:**

Zhen Li and group have studied the impedance spectroscopy characteristic of the perovskite-electrolyte interface-based devices.<sup>2</sup> They have compared two types of thin film fabrication techniques spin-coating (SC) and spray-deposition (SP) for MAPbI<sub>3</sub>, FA<sub>0.85</sub>CS<sub>0.15</sub>PbI<sub>3</sub> and MAPbBr<sub>3</sub> films in contact with a nonaqueous electrolyte composed of 0.1 M TBAPF<sub>6</sub> in CH<sub>2</sub>Cl<sub>2</sub>. The study reveals the role of thin film morphology and roughness in the performance of the liquid junction device which needs to be optimized. The fitting parameters obtained by them are summarized in the following table. The difference in the results from our study is because of different device structure, operating conditions and modelling parameters.

**Table S4.** Fitting parameters of EIS plot of SC-MAPbI<sub>3</sub> based devices.<sup>2</sup> Reprinted from Zhen Li.; Candy C. Mercado.; Mengjin Yang.; Ethan Palay.; and Kai Zhu.; Electrochemical impedance analysis of perovskite–electrolyte interfaces. *Chem. Commun.*, 2017, **53**, 2467–2470.

Diffusion element	R1 Ω	C2 F	R2 Ω	Diffusion element parameters			
				S2 Ωs <sup>-1/2</sup>	R3 Ω	t3 s	a3
RC	150	8E-5	360	-	-	-	-
Warburg	150	3E-5	200	9090	-	-	-
Anomalous	150	5E-5	240	-	700	4E-3	0.6

**Table S5.** Fitting parameters of the equivalent circuit to the Nyquist plots of the SC-MAPbI<sub>3</sub> sample at various applied potential.<sup>2</sup> Reprinted from Zhen Li.; Candy C. Mercado.; Mengjin Yang.; Ethan Palay.; and Kai Zhu.; Electrochemical impedance analysis of perovskite–electrolyte interfaces. *Chem. Commun.*, 2017, **53**, 2467–2470.

Applied potential (V vs. ref)	R1 Ω	C2 F	R2 Ω	Anomalous diffusion elements		
				R3 Ω	t3 s	a3
0.1	150	5E-5	240	700	4E-3	0.6
0.2	150	5E-5	245	552	3E-3	0.6
0.3	150	5E-5	264	300	2E-3	0.6

## References:

- 1 G. Y. Kim, A. Senocrate, T. Y. Yang, G. Gregori, M. Grätzel and J. Maier, *Nat. Mater.*, 2018, **17**, 445–449.
- 2 Z. Li, C. C. Mercado, M. Yang, E. Palay and K. Zhu, *Chem. Commun.*, 2017, **53**, 2467–2470.